

Modeling unsteady and perturbed combustion of heterogeneous composite propellants

G. Favale, F. Miccio *

Istituto di Ricerche sulla Combustione – C.N.R., P.le V. Tecchio 80, 80125 Napoli (I), Italy

Received 9 January 2006; received in revised form 2 February 2007; accepted 2 July 2007

Available online 28 July 2007

Abstract

The paper reports further developments of a numerical model for the combustion of composite solid propellants. Improvements include a better simulation of the fluid-dynamics by considering full Navier–Stokes equations coupled with species conservation, mass balance and energy balance equations. The model is also able to simulate the process under the action of an external perturbation, which is produced by a time-dependent heat flux impinging the propellant surface (e.g. laser source). Results of the model are reported in the paper in terms of two-dimensional distribution of most relevant variables, including gas concentration, velocity and temperature. The model has been validated against data of ignition delay available in the literature. The present study confirms that a simplified approach for fluid-dynamics is acceptable above a characteristic distance from the propellant surface, which is shortened at low values of the particle size and pressure. The analysis of model results under perturbed conditions demonstrates the pulsating impinging flux largely influences the propellant performance, the burning rate being largely increased by the irradiation. A periodic pulsating flux induces an oscillatory behavior of the burning process. At low perturbation frequency, the propellant is forced to burn at the same frequency of the external source. At high perturbation frequency, this effect disappears and typical fluctuations induced by the propellant heterogeneity are again evident. The transition between lower to higher frequencies (100–500 Hz) leads to emphasize the standard deviation of the observed time-dependent outputs (e.g. exit temperature), denoting the onset a resonance effect.

© 2007 Elsevier Masson SAS. All rights reserved.

Keywords: Heterogeneous propellants; Combustion; Modeling; Laser ignition

1. Introduction

The combustion of composite propellants is generally a time-dependent process with self-sustained oscillations in the regression rate and temperature [16]. The oscillatory character is related to the complex burning mechanism, which involves the propellant surface and leads to the occurrence of flames in the diluted phase. Therefore, it would be expected that the condensed phase heterogeneity plays a relevant role on the onset of the oscillatory combustion. During the last decade a large effort in numerical modeling of heterogeneous propellant combustion has been done by a number of investigators [4,7–9,11]. Miccio [9] firstly presented a two-dimensional (2D) numerical model able to account for a detailed topology of the solid phase. The model was based on a kinetic scheme including fuel pyroly-

sis, oxidizer decomposition, premixed and diffusion flames, and a simplified fluid-dynamics. Although some shortcuts are present, the model reasonably predicts the dynamic change of the propellant surface, as well as the distribution of gas species and temperature above the propellant. Knott and Brewster [7] implemented a combustion model based on the solution of the eigenvalue problem, after the introduction of a working variable following the Schwab–Zeldovich approach. Their model allows to calculate both temperature and species concentration fields, even if under the hypothesis of a very simplified kinetic scheme. The importance of considering the Navier–Stokes equations coupled with species conservation and energy equations in the 2D domain was addressed by Hegab et al. [4] They showed that the Oseen approximation (i.e. uniform velocity and constant density) leads to an acceptable error with respect to the full Navier–Stokes approach. In a further development of this latter study, Ramakrishna et al. [11] reported results of a model based on two diffusion flames with solution of Navier–Stokes

* Corresponding author. Tel.: +39-0815931567; fax: +39-0815931567.
E-mail address: miccio@irc.cnr.it (F. Miccio).

Nomenclature

c_i	stoichiometric coefficient	\bar{T}_{ex}	time averaged exit temperature
D	molecular diffusion coefficient	t	time
E	internal energy	t_{ign}	ignition time
f^c	inviscid flux (x axis)	\vec{U}	vector variable
f^v	viscous flux (x axis)	u	x component of gas velocity
G_i	generation rate	v	y component of gas velocity
g^c	inviscid flux (y axis)	x	axial coordinate
g^v	viscous flux (y axis)	y	transversal coordinate
L	transversal size of the propellant slab	Y_i	molar fraction
H_i	enthalpy of chemical reactions	α_b	thermal diffusivity of binder
m_b	binder mass	α_{ox}	thermal diffusivity of oxidizer
m_{ox}	oxidizer mass	γ	ratio between specific heats
\vec{n}	unitary vector	Δ	incremental operator
p	pressure,	λ	thermal conductivity for gas
R	gas-law constant	λ_b	thermal conductivity for binder
r	local regression rate	λ_{ox}	thermal conductivity for oxidizer
\bar{r}	average regression rate	μ	viscosity
q_i	reaction rate	Φ	frequency
S_b	binder surface	ρ	density
S_{ox}	oxidizer surface	σ	irradiation intensity
T	temperature	$\vec{\Sigma}$	vector variable
T_0	initial temperature	Ψ	standard deviation of temperature
T_{ex}	instantaneous exit temperature	Ω	control volume

equations under the hypothesis of constant Lewis and Prandtl numbers. They predicted non-planar regressing rate of the propellant surface and remarked the effect of the heat conduction in the condensed phase on the performance of the propellant. The extension to a three-dimensional scheme was recently proposed by Massa et al. [8], with the simulation of randomly-packed particles of ammonium perchlorate in a binder matrix. Their combustion model is able to predict the flow field and the 3D distribution of the combustion rate.

Studies into the application of a laser for increasing or controlling the combustion rate of composite propellants (e.g. ignition of cold propellants) are available in literature [10,15,17,18]. Rafi Ahmad et al. [10] reported their findings about tests of laser ignition for composite propellants. For visible laser wavelengths the adsorption of laser energy at surface propellant is roughly total, resulting in easy and reliable ignition at atmospheric pressure. Zanotti and Giuliani [17,18] studied the influence exerted by the radiation generated via a 70 W CO₂ laser on the ignition, extinction and propellant combustion behavior and extended the operation under the normal pressure deflagration limits. Pulsating/modulated lasers have also been used by Son and Brewster [15] as a perturbation agent. They proposed an analysis of the frequency response and remarked some non-linear effects at changing laser frequency. These experimental investigations provide a stimulus for modeling the propellant combustion under perturbed conditions.

The present paper deals with further developments and appliance of the previously published model [9] of composite propellants combustion. Major improvements are: (i) the im-

plementation and solution of the Navier–Stokes equations in the diluted phase for the determination of a fully developed unsteady 2D velocity field, (ii) the discrimination between oxidizer and binder regions in the condensed phase, as far as physical properties are concerned, (iii) a better simulation of the propellant ignition induced by an external energy source, (iv) the possibility to obtain the response under an imposed heat flux impinging the propellant surface. The paper describes these improvements and the related model results. Some intriguing trends shown by the model outputs under the action of a time-variable external perturbation are also discussed in the paper.

2. Modeling

The numerical model is an improvement of that presented by Miccio [9]. With reference to Fig. 1 reporting a sketch of the propellant during combustion, the oxidizer and binder species are simulated by adopting a rectangular multi-step grid. A single cell represents alternatively binder, oxidizer or gas. Six chemical species and five serial/parallel irreversible chemical reactions are considered. The latter include binder pyrolysis, oxidizer decomposition and flame reactions in the diluted phase. The kinetic rates depend on the partial pressure of the gaseous reactants, whereas the Arrhenius law provides the dependence on the temperature.

In the present study some simplifications of the previous model are removed. In particular, (i) oxidizer and binder have different properties (i.e. density, thermal conductivity and specific heat), (ii) the gaseous products of the heterogeneous re-

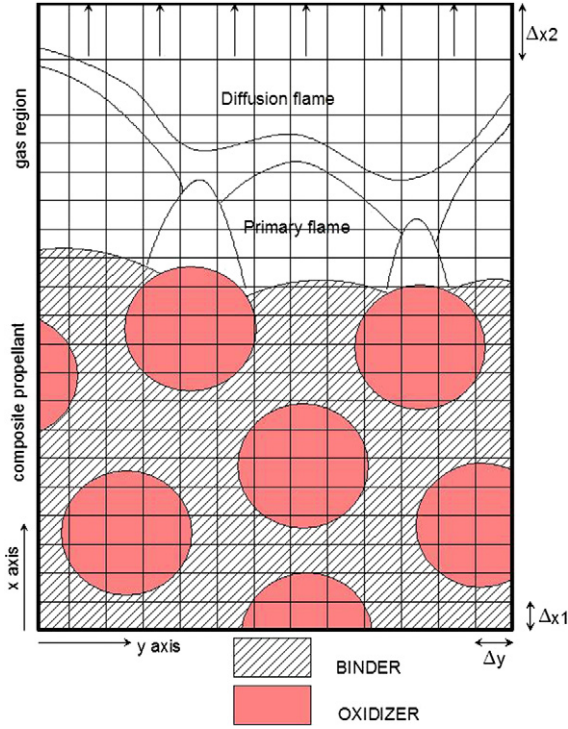


Fig. 1. A sketch of the simulated propellant with indication of flames and numerical grid.

actions depart from the propellant surface in normal direction, (iii) the fluid-dynamic field is two-dimensional, and (iv) gas viscosity is taken into account. Other relevant assumptions of the previous model are kept, namely validity of the gas law, low Mach number, neglecting the heat transfer by radiation. The latter assumption is valid in the limit of very short flames (i.e. lower than 1 mm) leading to a prevalent heat feedback to the exposed surface by conduction mechanism. Further details about modeling can be found in Miccio [9].

2.1. Equations

The model equations are reported below with reference to a system of orthogonal coordinates where the x axis is perpendicular to the propellant surface (axial direction) and y axis is transversal.

The equations for the solid phase are:

$$\frac{\partial m_s}{\partial t} = \int_{S_s} G_s dS \quad (1)$$

$$\frac{\partial T}{\partial t} = \alpha_s \left(\frac{\partial^2 T}{\partial x^2} + \frac{\partial^2 T}{\partial y^2} \right) \quad (2)$$

Eq. (1) is the global mass balance for the oxidizer and binder ($s = \text{ox}, \text{b}$), where the surface generation rate G_s is calculated according to Miccio [9]. The energy balance in the solid phase (Eq. (2)) takes into account the difference in the thermal diffusivity α_s of the two solid ingredients.

The equations for the dilute phase are the 2D compressible Navier–Stokes equations (Eq. (3))

$$\frac{\partial U}{\partial t} = \frac{\partial (f^c - f^v)}{\partial x} + \frac{\partial (g^c - g^v)}{\partial y} + \vec{\Sigma} \quad (3)$$

where $U = (\rho, \rho u, \rho v, \rho E)$ is the vector of conservative variables, f^c and g^c are the inviscid flux vectors for the x and y directions,

$$f^c = \begin{pmatrix} \rho u \\ \rho u^2 + p \\ \rho uv \\ u \left(\frac{\gamma}{\gamma-1} p + \frac{\rho}{2} (u^2 + v^2) \right) \end{pmatrix} \quad (4)$$

$$g^c = \begin{pmatrix} \rho v \\ \rho uv \\ \rho v^2 + p \\ v \left(\frac{\gamma}{\gamma-1} p + \frac{\rho}{2} (u^2 + v^2) \right) \end{pmatrix} \quad (5)$$

f^v and g^v are the viscous flux vectors for the x and y directions,

$$f^v = \begin{pmatrix} 0 \\ \mu \left(\frac{4}{3} \frac{\partial u}{\partial x} - \frac{2}{3} \frac{\partial v}{\partial y} \right) \\ \mu \left(\frac{\partial u}{\partial y} + \frac{\partial v}{\partial x} \right) \\ \mu \left[u \left(\frac{4}{3} \frac{\partial u}{\partial x} - \frac{2}{3} \frac{\partial v}{\partial y} \right) + v \left(\frac{\partial u}{\partial y} + \frac{\partial v}{\partial x} \right) \right] + \lambda \frac{\partial T}{\partial x} \end{pmatrix} \quad (6)$$

$$g^v = \begin{pmatrix} 0 \\ \mu \left(\frac{\partial u}{\partial y} + \frac{\partial v}{\partial x} \right) \\ \mu \left(\frac{4}{3} \frac{\partial v}{\partial y} - \frac{2}{3} \frac{\partial u}{\partial x} \right) \\ \mu \left[v \left(\frac{4}{3} \frac{\partial v}{\partial y} - \frac{2}{3} \frac{\partial u}{\partial x} \right) + u \left(\frac{\partial u}{\partial y} + \frac{\partial v}{\partial x} \right) \right] + \lambda \frac{\partial T}{\partial y} \end{pmatrix} \quad (7)$$

and the generation term $\vec{\Sigma} = [0, 0, 0, \sum_i q_i H_i]$ is again computed according to Miccio [9].

The conservation equation for the generic species ($i = B, D, E$ and F) in the diluted phase reads:

$$\frac{\partial Y_i}{\partial t} = -u \frac{\partial Y_i}{\partial x} - v \frac{\partial Y_i}{\partial y} + \frac{\partial}{\partial x} \left(D \frac{\partial Y_i}{\partial x} \right) + \frac{\partial}{\partial y} \left(D \frac{\partial Y_i}{\partial y} \right) + G_i \quad (8)$$

The trivial condition regarding the sum of molar fractions $\sum_i Y_i = 1$ applies. G_i is the generation term for the generic species i by chemical reactions. Further details concerning the reactions and kinetics are reported in Miccio [9].

The viscosity μ of the fluid is computed by means of the Sutherland's formula [3].

$$\mu = 1.458 \times 10^{-6} \frac{T^{1.5}}{110.4 + T} \quad (9)$$

2.2. Boundary conditions

The derivatives with respect to x axis of molar fractions, $\partial Y_i / \partial x$, and temperature, $\partial T / \partial x$, are set to zero at infinity from the propellant surface ($x \rightarrow \infty$). At the cold end of the propellant ($x = 0$) the derivatives of the temperature are set equal to zero, $\partial T / \partial x = 0$. Similarly, the derivatives with respect to y axis, $\partial Y_i / \partial y$ and $\partial T / \partial y$, are set to zero along the lateral edges of the propellant (i.e. $y = \pm L/2$).

At the propellant surface, the following equations are imposed: species conservation (Eq. (10)), continuity of the temperature ($T_s = T_g$ for $s = \text{ox}, \text{b}$), continuity of the thermal flux (Eq. (11) for $s = \text{ox}, \text{b}$), and state equation applied to the volumetric flow rate of the departing gas (Eqs. (12)–(13)).

$$D \frac{\partial Y_i}{\partial n} = -G_i \quad (10)$$

$$\lambda_g \frac{\partial T}{\partial n} = \lambda_s \frac{\partial T}{\partial n} - \sum_i G_i H_i \quad (11)$$

$$u = n_x \frac{RT}{p} \sum_i c_i G_i \quad (12)$$

$$v = n_y \frac{RT}{p} \sum_i c_i G_i \quad (13)$$

2.3. Initial conditions

At the initial time ($t = 0$) the molecular fractions of gaseous species are set to zero ($Y_i = 0$) except for the inert species F ($Y_F = 1$). The temperature is set to T_0 , the gas velocity is null ($u, v = 0$), and the properties in the condensed phase are assigned, according to the topological description of the propellant.

2.4. Discretization

The solution of model equations has been pursued via a numerical approach by introducing a topological rectangular matrix (Fig. 1) representing a limited propellant region with transversal size in the range 200–400 μm and a few millimeters high. Periodicity of lateral boundaries are imposed. Each element can assume a discrete value 0, 1, 2 for indicating the presence of binder, oxidizer, or gas, respectively. The numerical grid of the matrix could adopt different steps for x and y axes in the range 2–10 μm . In addition, far from the propellant surface the mesh is 10 times larger along x axis for the simulation of the gas-phase. The derivatives with respect to time and space are numerically computed using an explicit method with first order accuracy for the time and second order accuracy for the space [1].

To solve the 2D compressible Navier–Stokes equations we use the finite volume method, which is based on an integral formulation taking into account a quadrilateral control volume Ω with a northern, southern, eastern and western interfaces. The explicit Euler method has been applied for the discretization of this term (Eq. (16)).

$$U_{i,j}^{n+1} = U_{i,j}^n - \frac{\Delta t}{\Delta x \Delta y} \left(\sum_{s \in \{N, S, E, W\}} ((f^c - f^v)^n \Delta x + (g^c - g^v)^n \Delta y)_s \right) \quad (14)$$

The derivatives that appear in the viscous fluxes are centrally discretized. The inviscid numerical fluxes are determined with a second order accuracy scheme, adopting the flux-vector splitting method of Van-Leer [6].

Table 1
Physical and chemical data

Density – oxidizer	kg m^{-3}	1650
Density – binder	kg m^{-3}	1270
Thermal conductivity – oxidizer	$\text{W m}^{-1} \text{K}^{-1}$	0.34
Thermal conductivity – binder	$\text{W m}^{-1} \text{K}^{-1}$	0.17
Thermal diffusivity – oxidizer	$\text{m}^2 \text{s}^{-1}$	2.2×10^{-7}
Thermal diffusivity – binder	$\text{m}^2 \text{s}^{-1}$	1.4×10^{-7}
Oxidizer/binder ratio (by mass)	–	3
Particle size of oxidizer (DPP)	μm	110
Binder slice width (SP)	μm	50
Binder pyrolysis pre-exponential factor	$\text{mol m}^{-2} \text{s}^{-1}$	1.0×10^4
Binder pyrolysis activation energy	J mol^{-1}	63 000
Oxidizer decomposition pre-exponential factor	$\text{mol m}^{-2} \text{s}^{-1}$	1.0×10^7
Oxidizer decomposition activation energy	J mol^{-1}	92 000
Oxidizer flame pre-exponential factor	$\text{mol m}^{-3} \text{s}^{-1}$	1.0×10^{-1}
Oxidizer flame activation energy	J mol^{-1}	90 000
Diffusion flame pre-exponential factor	$\text{mol m}^{-3} \text{s}^{-1}$	1.0×10^{-2}
Diffusion flame activation energy	J mol^{-1}	62 700
Adiabatic temperature	K	2700

Finally, the numerical procedure adopts an integration step with respect to the time that is self-variable, checking for the stability of the solution, resulting in an average step of around 10^{-8} s during the simulations.

2.5. Properties of the propellant

Ammonium perchlorate and HTPB (hydroxyl-terminate polybutadiene) are considered in this study as ingredients for the composite propellants, in two different configurations, sandwich propellant (SP) and dispersed particle propellant (DPP), with the same overall oxidizer/binder mass ratio. Values of physical and chemical data used for calculations are reported in Table 1, according to the available literature [2,5,9,12]. Established correlations are used to evaluate the dependencies of λ , E and D on the temperature and pressure [14].

3. Results

Fig. 2 shows a series of snapshots representing the propellant as predicted by the model, for the SP configuration (Fig. 2(a)) and DPP configuration (Figs. 2(b), 2(c), and 2(d)). In both cases, the surface is not flat as a consequence of the non-uniformity in the local regression rate r . The higher r , the deeper is the surface depression. For sandwich propellant the surface shape does not change significantly after the ignition, whereas for dispersed particles propellant the surface shape is time-dependent and highly corrugated. The influence of the pressure is also large, as clearly shown by the comparison of panels *b* and *d*, which are referred at $p = 3$ and 6 MPa, respectively. The depth of the surface layer consistently increases as the pressure augments. The streamlines of the velocity field computed by the model are also reported in all panels of Fig. 2.

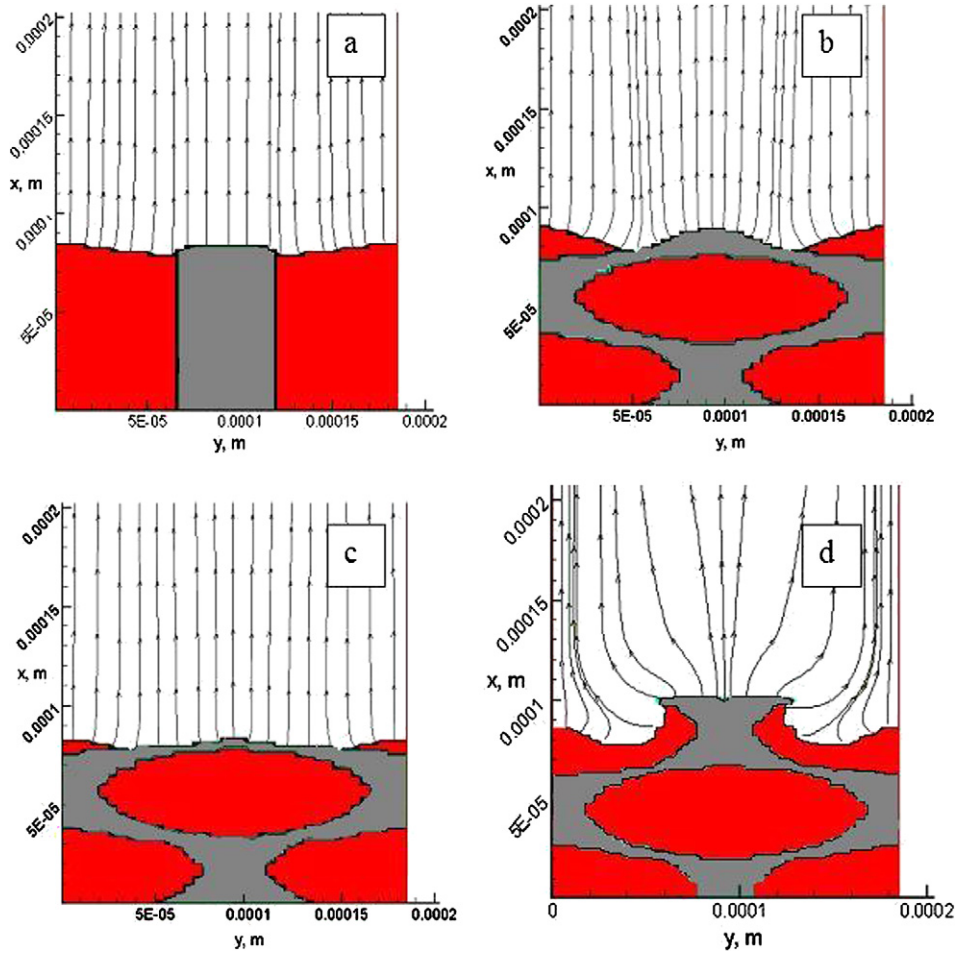


Fig. 2. Snapshots of the propellant showing the streamlines of the velocity field after the ignition: (a) sandwich propellant ($p = 3$ MPa), (b), (c) dispersed-particle propellant at two different times ($p = 3$ MPa), (d) dispersed-particle propellant ($p = 6$ MPa).

It clearly appears that the streamlines are not straight in the proximity of the propellant, as a consequence of the corrugated surface. They depart orthogonal to the local surface profiles and tend to be parallel at the top of simulated domain. This represents a major difference with respect to the estimates of the previous model by Miccio [9] where the transversal component of the velocity are always considered null. Therefore, the model does not fail during the simulation of the surface evolution leading in some particular cases to the formation of craters, crevices or spills of materials near the binder–oxidizer interface as sketched in Fig 2(d). Although this morphology appears quite unrealistic, it demonstrates the model is robust and reliable also for simulation of strange surface profiles established after ignition. DPP scheme leads to a more accentuated curvature of the streamlines as a consequence of the generated craters and hills along the propellant surface. However, the velocity field results mono-dimensional for both schemes in a large portion of the gas-phase domain (i.e. for x greater than 0.200 mm at $p = 3$ MPa). In fact, the transversal components are negligible and the streamlines become nearly parallel above this elevation. It is worth noting that this characteristic distance has the same order of magnitude of the propellant characteristic length (e.g. oxidizer particle size). Again, the pressure exerts a large influence on the streamlines curvature and, in turn, on the dis-

tance after which the flow becomes mono-dimensional, such a distance being increased by a factor 5 as p passes from 3 to 6 MPa.

Fig. 3 reports the time profiles of three average temperatures along y axis (panel b) and the average regression rate $\bar{r} = \int_{S_{ox}+S_b} r dS$ (panel c) during a simulation carried out at $p = 3$ MPa for a sandwich propellant. The ignition occurs by means of an external heat flux that impinges the surface. Its intensity and duration are 10^7 W m^{-2} and 5 m s, respectively, as indicated in Fig. 3(a). The surface temperature (curve 1 in panel (b)) slightly increases after the ignition and, in turn, an augmentation of the regression rate is noted in Fig. 3(c). It also appears that the regression rate is two times higher during the external irradiation of the propellant surface. Afterwards there is a sudden drop and a further increase that is induced by the onset of the flame reactions in the gas phase. The average temperatures at the middle ($z = 1.14$ mm) and the end ($z = 3.6$ mm) of the gas-phase region progressively increase until rather constant values are achieved after 25 m s.

As above, the time profiles of the average temperatures (Fig. 4(b)) and the surface regression rate (Fig. 4(c)) are plotted for a dispersed particle propellant under same burning conditions. Again the surface temperature (curve 1 in panel (b)) slightly increases as a consequence of the propellant ignition.

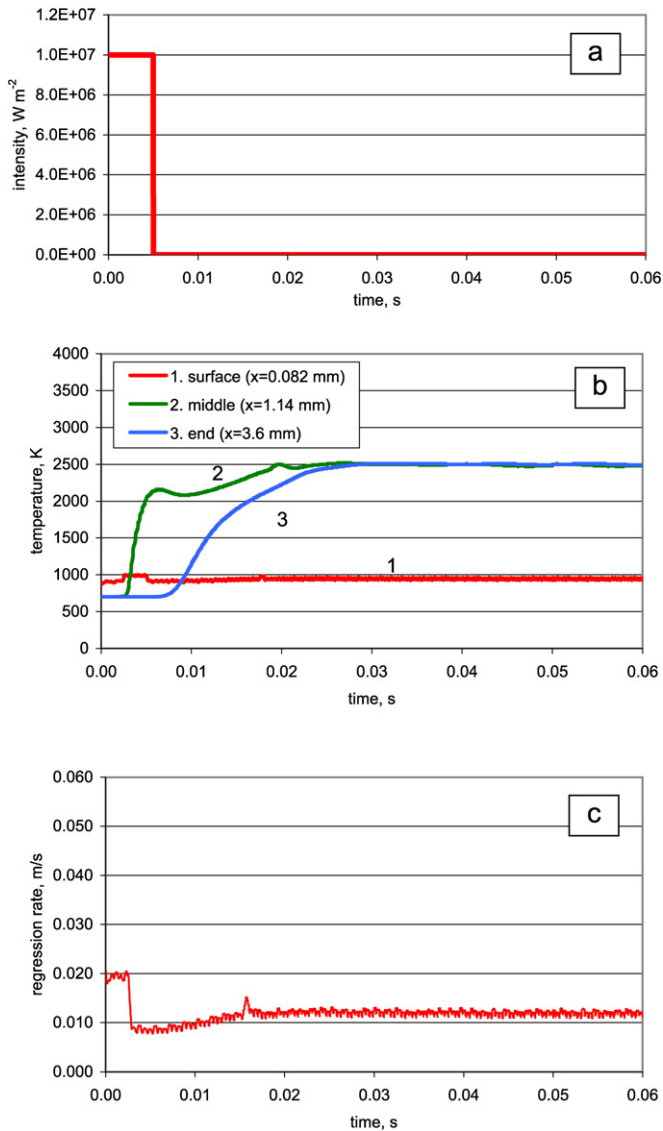


Fig. 3. Transient profiles of model variables (sandwich propellant $p = 3$ MPa): (a) intensity of the imposed heat flux, (b) average temperatures at three axial levels, (c) average regression rate.

The regression rate (Fig. 4(c)) exhibits a non-steady behavior with repeated and almost regular peaks. This is an obvious consequence of the intrinsic heterogeneity in the condensed phase. The oxidizer particles belonging to the frontier zone are progressively consumed whereas fresh ones are newly exposed for reactions. Therefore, a periodic transition between oxidizing rich conditions and fuel rich conditions locally takes place. However, the burning process proceeds and no extinction occurs, even in presence of an oscillatory behavior. The fluctuations in the regression rate also affect the profiles of the average temperatures downstream (Fig. 4(b)) that fluctuate upon a time of nearly 10 ms around a stable average value. By comparison of Figs. 3 and 4 it also appears that on the whole the regression rate and temperatures are higher for the DPP scheme, the mixing of gaseous reactants being promoted under the constrain of equal oxidizer/binder mass fraction in both propellants. In contrast, a comparison based on the equality of characteristic

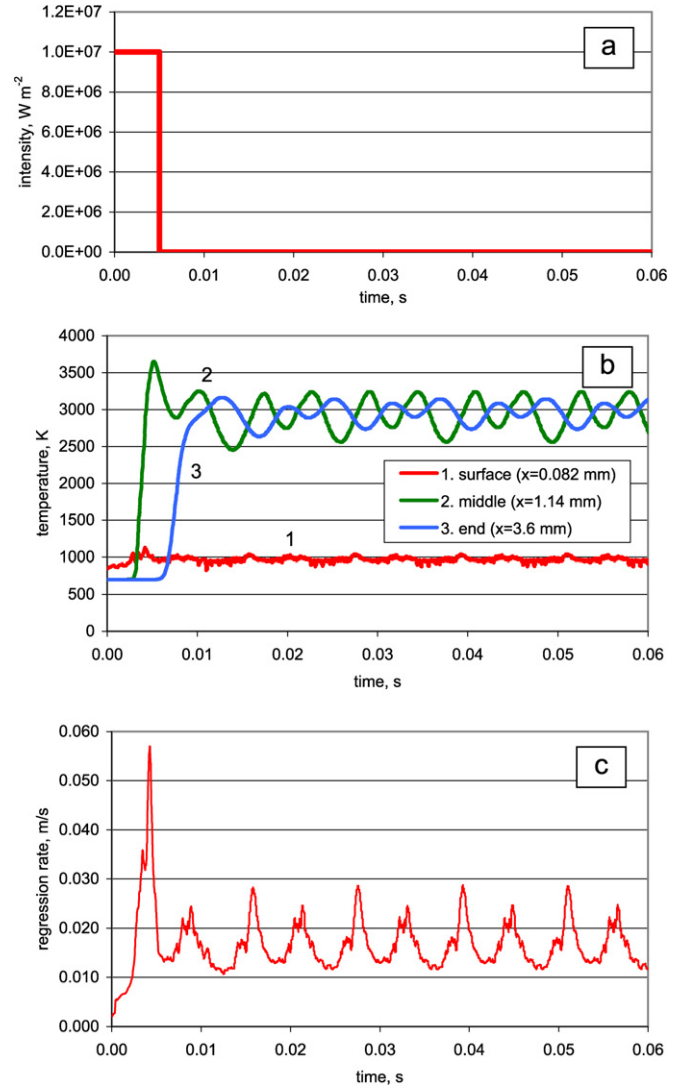


Fig. 4. Transient profiles of model variables (dispersed particle propellant $p = 3$ MPa): (a) intensity of the imposed heat flux, (b) average temperatures at three axial levels, (c) average regression rate.

length-scale would be favorable to sandwich propellant, since the uninterrupted and stable contact between the two ingredients leads to a higher regression rate.

Fig. 5 reports the results of the calculations for DPP scheme under an external forcing irradiation, which is pulsating as reported in the panel a, corresponding to a positive square wave with constant frequency Φ . The spontaneous fluctuations shown in the previous Fig. 4 for temperatures and regression rate are emphasized by the action of the pulsed impinging flux. Further and more intense peaks appear in the regression rate curve (Fig. 5(c)), as a consequence of the transitions between null to positive levels of the flux intensity. The time average values of temperatures and regression rate also increase, by virtue of the additional energy supplied by the pulsating impinging irradiation.

The flame structure above the propellant surface is reported in Fig. 6 for a simulation executed under pulsating laser irradiation ($\Phi = 1000$ Hz). The panels of Fig. 6 show the two-

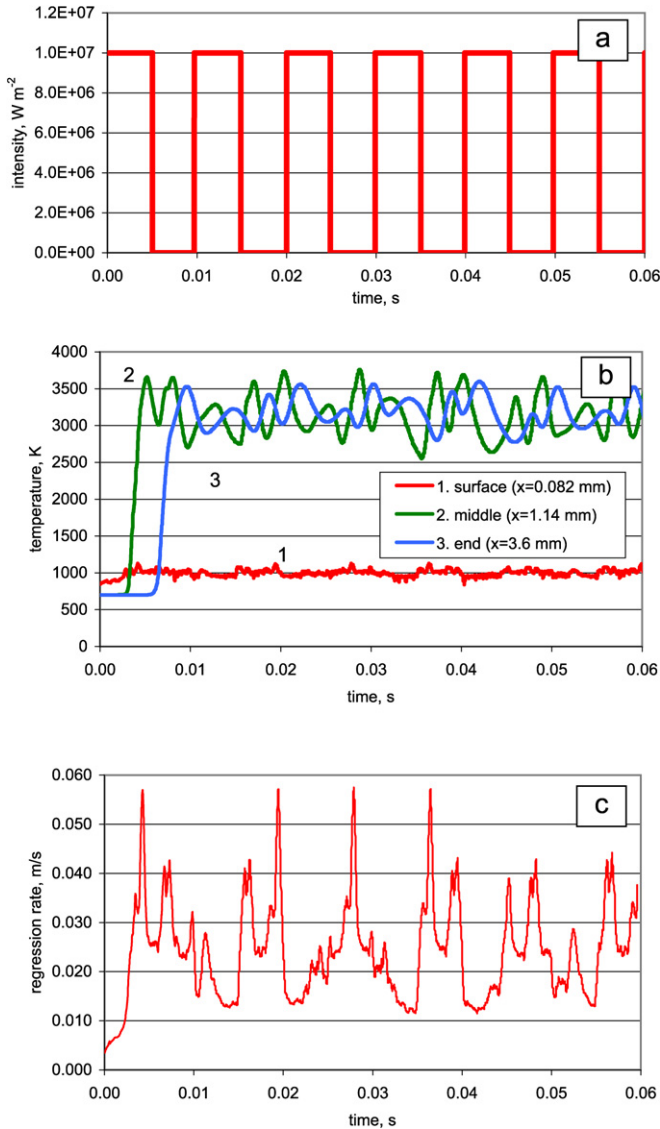


Fig. 5. Transient profiles of model variables (dispersed particle propellant $p = 3$ MPa): (a) intensity of the imposed heat flux, (b) average temperatures at three axial levels, (c) average regression rate.

dimensional distribution for the chemical species F , B , E and for the temperature, where F is the final product, B the product of binder pyrolysis and E an oxidizer decomposition product. The top panels refer to “laser-on” conditions whereas the bottom panels to absence of irradiation (laser-off). The typical structure of a diffusion flame can be observed above the oxidizer particle, since the reactants diffuse in transversal direction and form a plume. The temperature approaches the adiabatic value far from the surface and exhibits a flat profile in transversal direction as a consequence of the small size of propellant grains. A difference can be easily noted between the flame length when laser is ON and OFF. In fact, the flame is significantly shorter in absence of the impinging flux thanks to the lower axial velocity of gaseous species departing from the propellant surface.

Fig. 7 reports the ignition delay at atmospheric pressure ($p = 10^5$ Pa) for a simulated sandwich propellant as a function

of the impinging flux intensity σ . The higher the flux intensity, the lower the ignition delay. In the same figure data points taken from Rafi Ahmad and Russell [10] are reported for comparison. Although uncertainties about geometrical and physical parameters have to be taken into account, the rather good agreement between experimental data and model estimates demonstrates the model assumptions as well as the choice of parameters are quite reasonable.

The exit temperature T_{ex} was processed in order to compute the time average value \bar{T}_{ex} and standard deviation Ψ after the ignition ($t > 10$ ms). These outputs are plotted in Fig. 8 as a function of the frequency Φ of the pulsating flux. The average temperature \bar{T}_{ex} shows a non-monotone dependence on Φ . An increase is firstly noted until a maximum value is achieved at $\Phi = 200$ Hz; then the average temperature decreases and tends to an asymptotic value, as Φ increases. As far as the standard deviation is concerned, at low frequency it attains very large values. Increasing the frequency, Ψ exhibits a decreasing trend and achieves an asymptotic value at high frequency. Again, in the intermediate range 100–1000 Hz, the standard deviation shows a local maximum that is strictly related to that of the \bar{T}_{ex} curve.

In order to better understand the role exerted by the frequency Φ of the imposed irradiation, an analysis was carried out in the frequency domain. A parametric reconstruction was performed for the variable T_{ex} (see Figs. 3 and 4) based on three sinusoidal functions [13]. Among these, the dominant sinusoidal function was selected to characterize the signal of T_{ex} variable. Results of this analysis are reported in Fig. 9, where the dominant frequency is plotted against the frequency of the imposed irradiation. A curve with ordinate equal to abscissa has also been superposed in the diagram in order to see where the calculated results depart from the linear dependence on the frequency of the pulsating laser. The two curves are close in the interval 25–250 Hz. An intersection is located at $\Phi = 250$ Hz, and afterwards the curves follow different paths. The steadily increase of the dominant frequency on the left side of the diagram ($\Phi = 25$ –500 Hz) is an obvious consequence of the influence exerted by the imposed pulsating irradiation on the surface temperature of the propellant. In fact, the impinging flux forces the propellant to burn in an oscillatory mode in phase with the imposed frequency. On the right side of the diagram, the dominant frequency achieves the asymptotic value of around 250 Hz. This latter should be interpreted as the spontaneous frequency of oscillation when the combustion takes place at a self-sustained regression rate, not only T_{ex} fluctuating but also all other relevant variables. In other words, when the frequency of the perturbing irradiation is large enough (i.e. 500–10 000 Hz), the dominant frequency is determined by the periodic process of depletion of oxidizer particles located along the propellant surface, replacement with new oxidizer grains and burnout of the binder thickness between contiguous particles. For present calculations, this frequency can be roughly estimated as the ratio between the actual average regression rate and the particle size giving a value of around 220 Hz, which is very close to the asymptotic value of Fig. 9. In contrast, as the frequency of the perturbing irradiation approaches the spontaneous frequency of

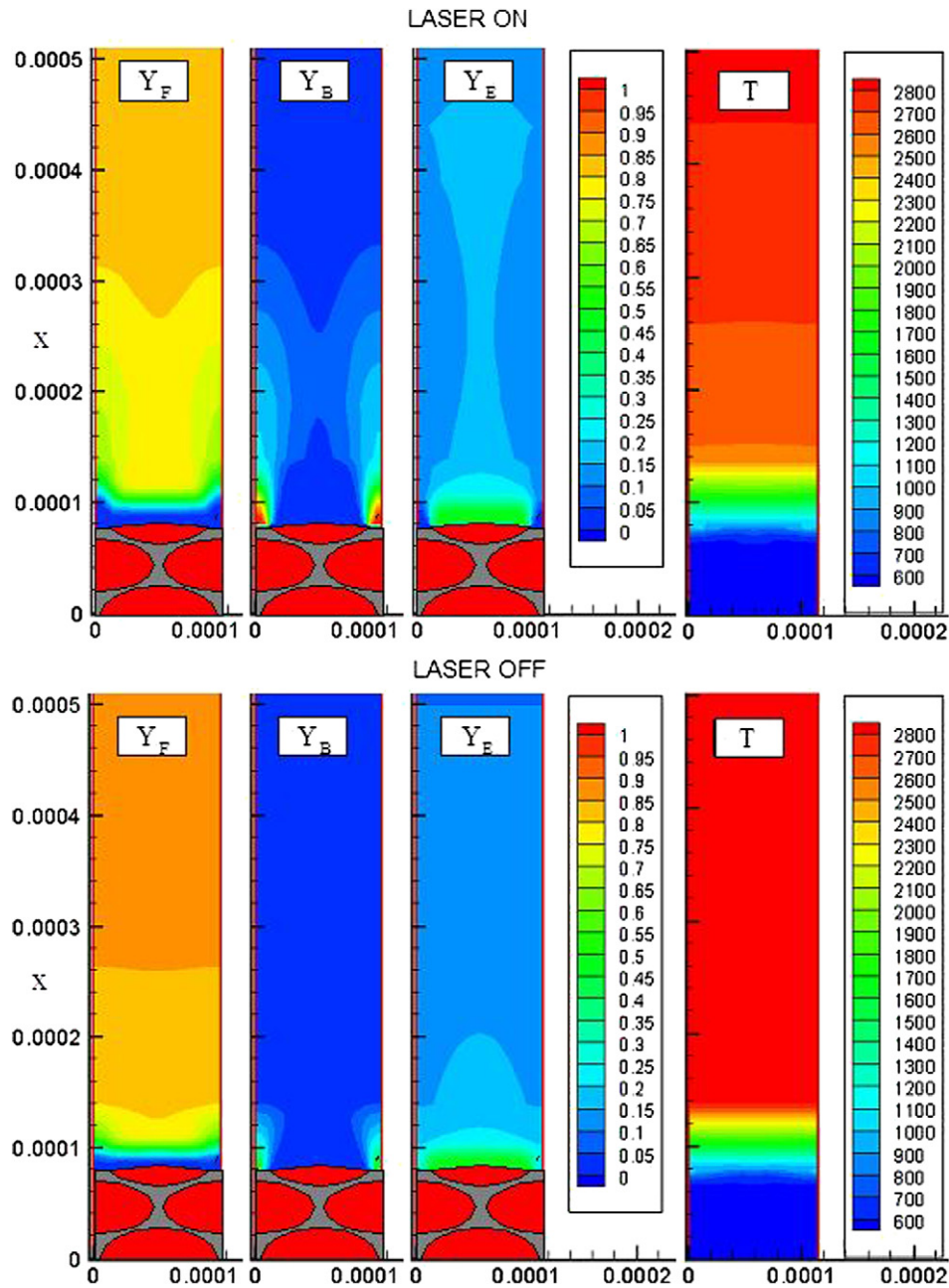


Fig. 6. Two-dimensional distribution of gaseous species (F , B , E) and temperature in the simulated domain during a run carried out under perturbed conditions ($\sigma = 10^7 \text{ W m}^{-2}$, $\Phi = 1000 \text{ Hz}$, $p = 3 \text{ MPa}$).

the system (i.e. intermediate range of Fig. 9) a resonance effect takes place, since higher fluctuations in temperature T_{ex} and a local maximum in Ψ are correspondingly shown in Fig. 8.

4. Conclusion

A numerical model for the combustion of composite propellants has been developed for the simulation under dynamic conditions. The model allows the calculation of the surface shape and gas streamlines, as well as distribution of temperature and gas concentration. Another feature is the possibility to describe the propellant evolution under an imposed heat flux impinging

the propellant surface. The model has been successfully validated against data of ignition delay available in the literature.

The predicted shape of the propellant surface is not flat for both sandwich and dispersed particle propellants. For dispersed particle propellant the shape is also largely time dependent. The pressure has a significant influence on the shape and depth of the surface layer. The streamlines of the velocity field are not straight in the proximity of the propellant surface, but tend to be axial and parallel as the distance from the propellant increases. In general, the transversal components are negligible after a few particle sizes from the surface, although the pressure is also relevant to determine this characteristic distance. This result can be regarded as a limit for the utilization of the

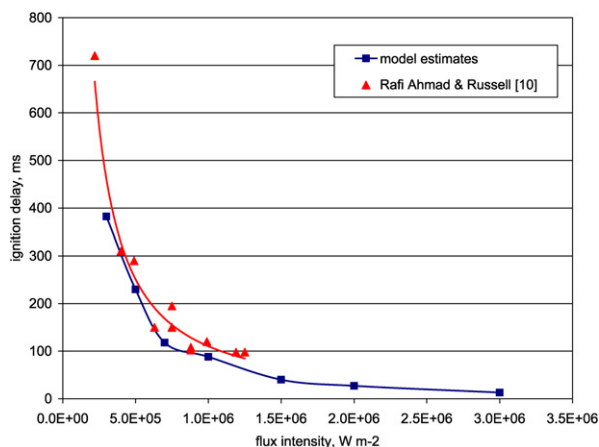


Fig. 7. Ignition delay as a function of the laser irradiation intensity ($p = 10^5$ Pa).

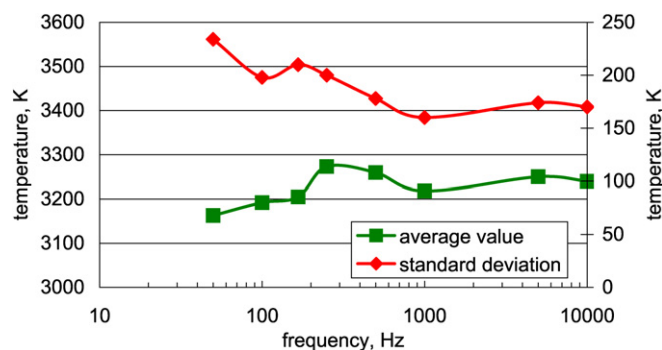


Fig. 8. Time average value and standard deviation of the exit temperatures after the ignition versus the frequency of the impinging irradiation (DPP, $t_{\text{ign}} = 5$ ms, $\sigma = 10^7$ W m $^{-2}$, $p = 3$ MPa).

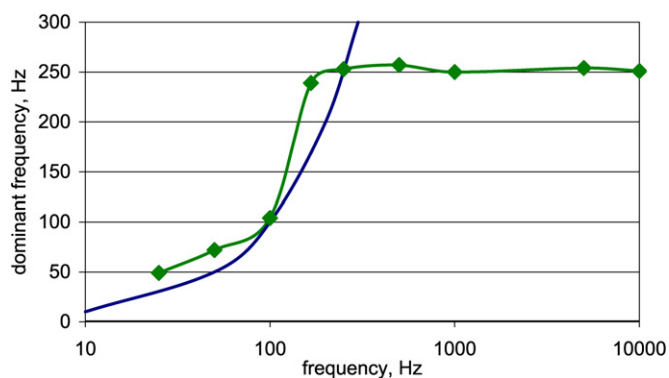


Fig. 9. dominant frequency of the exit temperatures after ignition versus the frequency of the impinging irradiation (DPP, $t_{\text{ign}} = 5$ ms, $\sigma = 10^7$ W m $^{-2}$, $p = 3$ MPa).

Oseen approximation in numerical modeling of composite propellant combustion.

After the ignition, the model outputs exhibit a spontaneous oscillatory behavior in the case of dispersed particle propellants. The regression rate is non-steady with repeated and almost regular peaks, as an obvious consequence of the intrinsic heterogeneity in the condensed phase. This behavior is confined

at the geometrical scale of the particle size in the condensed phase, but is also propagated in the diluted phase.

Under perturbed conditions, fluctuations in the calculated variables are emphasized by the action of the pulsating external radiation. So far, a non-monotone response of the model is observed. The frequency analysis shows that the propellant follows the perturbation frequency at low values of this latter, and exhibits a spontaneous frequency during combustion, at high values of the perturbation frequency. As the frequency of the perturbing irradiation approaches the spontaneous propellant frequency, a resonance effect takes place leading to higher fluctuations in model outputs. This finding deserves further consideration for appliances in controlling the propellant combustion rate.

Acknowledgements

The present research was funded by Italian Space Agency. Prof. L. De Luca is gratefully acknowledged for its support and collaboration.

References

- [1] J.D. Anderson, Explicit finite difference methods: some selected applications to inviscid and viscous flows, in: J.F. Wendt (Ed.), Computational Fluid Dynamics: An Introduction, Springer-Verlag, Berlin, 1996 (Chapter 7).
- [2] M.W. Beckstead, R.L. Derr, C.F. Price, A model of composite solid-propellant combustion based on multiple flames, *AIAA J.* 8 (1970) 2200–2207.
- [3] R.F. Grasso, C. Meola, Euler and Navier–Stokes equations for compressible flows: finite-volume methods, in: R. Peyret (Ed.), Handbook of Computational Fluid Mechanics, Academic Press, London, 1996 (Chapter 4).
- [4] A. Hegab, T.L. Jackson, J. Buckmaster, D.S. Stewart, Nonsteady burning of periodic sandwich propellants with complete coupling between the solid and gas phases, *Combust. Flame* 125 (2001) 1055–1070.
- [5] C.E. Hermance, A model of composite propellant combustion including surface heterogeneity and heat generation, *AIAA J.* 9 (1966) 1629–1637.
- [6] K.A. Hoffmann, S.T. Chiang, Computational Fluid Dynamics, vol. II, fourth ed., EESbooks, Wichita, KS 2000 (Chapter 12).
- [7] G.M. Knott, M.Q. Brewster, Two-dimensional combustion modeling of heterogeneous solid propellants with finite Peclet number, *Combust. Flame* 121 (2000) 91–106.
- [8] L. Massa, T.L. Jackson, M. Short, Numerical solution of three-dimensional heterogeneous solid propellants, *Combust. Theory Modelling* 7 (2003) 579–602.
- [9] F. Miccio, Numerical modelling of composite propellant combustion, *Proc. Combustion Institute* 27 (1998) 2387–2395.
- [10] S. Rafi Ahmad, D.A. Russell, C.J. Leach, Studies into laser ignition of unconfined propellants, *Propellants, Explosives, Pyrotechnics* 23 (2001) 235–245.
- [11] P.A. Ramakrishna, P.J. Paul, H.S. Mukunda, Sandwich propellant combustion: modeling and experimental comparison, *Proc. Combustion Institute* 29 (2002) 2963–2973.
- [12] K.N.R. Ramohalli, Steady-state burning of solid propellants under zero cross flow situation, in: K.K. Kenneth, M. Summerfield (Eds.), Fundamentals of Solid-Propellant Combustion, in: Progress in Astronautics and Aeronautics, vol. 90, AIAA, New York, 1984, pp. 409–477.
- [13] J.N. Rayner, An Introduction to Spectral Analysis, Pion Limited, London, 1971 (Chapter 2).
- [14] R.C. Reid, J.M. Prausnitz, B.E. Poling, The Properties of Gases and Liquids, McGraw-Hill Book Comp., New York, 1987 (Chapters 10–11).
- [15] S.F. Son, M.Q. Brewster, Unsteady combustion of homogeneous energetic solids using the laser-recoil method, *Combust. Flame* 100 (1995) 283–291.

- [16] C. Zanotti, U. Carretta, C. Grimaldi, G. Colombo, Self-sustained oscillatory burning of solid propellants: experimental results, in: L. De Luca, E.W. Price, M. Summerfield (Eds.), *Nonsteady Burning and Combustion of Solid Propellants*, in: *Progress in Astronautics and Aeronautics*, vol. 143, AIAA, New York, 1992, pp. 399–439.
- [17] C. Zanotti, P. Giuliani, Pressure deflagration limit of solid rocket propellants: experimental results, *Combust. Flame* 98 (1994) 35–45.
- [18] C. Zanotti, P. Giuliani, Composite propellant ignition and extinction by CO₂ laser at subatmospheric pressure, *Propellants, Explosives, Pyrotechnics* 23 (1998) 254–259.